Supplementary Material

The MCL-1 BH3 Helix is an Exclusive MCL-1 inhibitor and Apoptosis Sensitizer

Michelle L. Stewart, Emiko Fire, Amy E. Keating, and Loren D. Walensky

SUPPLEMENTARY METHODS

Anti-apoptotic protein production. Transformed *Escherichia coli* BL21 (DE3) were cultured in ampicillin-containing Luria Broth and protein expression was induced with 0.5 mM isopropyl β-D-1-thiogalactopyranoside (IPTG). The bacterial pellet was resuspended in buffer (250 mM NaCl, 20 mM Tris, complete protease inhibitor tablet, pH 7.2), sonicated, and after centifugation at 45,000x*g* for 45 minutes, the supernatant was applied to a glutathione-agarose (Sigma) column and washed with PBS. On-bead digestion of GST-tagged proteins was accomplished by overnight incubation at room temperature in the presence of thrombin (75 units) in PBS (3 mL), and the cleaved proteins were purified by size exclusion chromatography (SEC) using 150 mM NaCl, 50 mM Tris, pH 7.4 buffer conditions.

Cytochrome *c* release assays. Isolated mouse liver mitochondria (0.5 mg/mL) were incubated at 37°C for 40 minutes in the presence of a serial dilution of MCL-1 $SAHB_D$, singly or in combination with BID BH3 peptide. The pellet and supernatant fractions were isolated by centifugation, and cytochrome *c* was

quantitated using a colorimetric ELISA assay (R&D Systems). Percent cytochrome *c* released into the supernatant (%cytoc_{sup}) from releasable mitochondrial pools was calculated according to the following equation: %cyto*c*=[(cytoc_{sup}-cytoc_{backgr})/(cytoc_{total}-cytoc_{backgr})]*100, where background release represents cytochrome *c* detected in the supernatant of vehicle-treated samples and total release represents cytochrome *c* measured in 1% Triton-X 100 treated samples.

MCL-1 SAHB photocrosslinking. OPM2 cellular lysates were generated by vortexing cells (1 x 10^7) with ice cold Buffer A (50 mM Tris pH 7.4, 150 mM NaCl, 1% CHAPS, 1mM EDTA, 1.5 mM $MgCl_2$, EDTA-free complete protease inhibitor cocktail [Roche]), followed by incubation on ice for 10 minutes and collection of the supernatant by centrifugation. After pre-clearing the supernatant for 1 hour with high capacity streptavidin agarose (Pierce) at 4°C, lysates were incubated with MCL-1 $SAHB_D$ (10 μM) or MCL-1 $pSAHB_D$ (10 μM) and irradiated with 365 nm ultraviolet light for 3 hours. Unreacted peptide was removed by overnight dialysis at 4°C in Buffer B (200 mM NaCl, 50 mM Tris pH 7.4) using 6-8 kD molecular weight cut-off D-Tube dialyzers (EMD Biosciences). After addition of SDS to a final concentration of 0.2%, biotin capture was achieved by incubation with high capacity streptavidin agarose (50 μL 50% slurry/reaction) for 2 hours at room temperature. The streptavidin beads were successively washed (3x) at room temperature in 1% SDS in PBS, 1 M NaCl in PBS, and then 10% ethanol in PBS. Proteins crosslinked to the biotinylated peptide were eluted by boiling for

30 minutes in a 10% SDS solution (Promega) containing D-biotin (10 mg/mL), electrophoresed using 4%–12% gradient Bis-Tris gels (Invitrogen), and then subjected to MCL-1 western analysis (S19 antibody, Santa Cruz Biotechnology).

Cellular uptake assay. OPM2 cells (4×10^6) were incubated with vehicle or FITC-SAHB (40 μM) in Opti-MEM medium (Invitrogen) at 37ºC for 1.5 hours in the dark. Cells were washed once with PBS, incubated with 0.25% trypsin for 5 minutes, washed twice with PBS, and lysed on ice with 200 μL cold Triton X-100 lysis buffer (50 mM Tris pH 7.4, 150 mM NaCl, 1 mM EDTA, 1 mM DTT, 0.1% Triton X-100, complete protease inhibitor pellet). Cellular debris was pelleted at 14,000x*g* for 10 minutes at 4ºC and the supernatant was collected, electrophoresed, and subjected to fluorescence imaging using a Typhoon 9400 (GE Healthcare Life Sciences).

Supplementary Table 1 BH3 peptide compositions.

Peptide	Sequence	N-terminus	MW	M/3
Figure 1: Identification of an MCL-1-selective BH3 domain.				
BIM SAHB$_A$	IWIAQELRXIGDXFNAYYARR	FITC-βAla-	3064	1022.5
BID SAHB$_A$	DIIRNIARHLAXVGDXBDRSI	FITC-βAla-	2856	953.2
BAD SAHB$_A$	NLWAAQRYGRELRXBSDXFVDSFKK	FITC-βAla-	3058	1020.0
NOXA SAHB$_A$	LEVESATQLRXFGDXLNFRQKL	FITC-βAla-	3073	1025.8
PUMA SAHB$_A$	QWAREIGAQLRXBADXLNAQY	FITC-βAla-	2925	976.0
BAK SAHB$_A$	QVGRQLAXIGDXINRRYD	FITC-βAla-	2583	862.0
BAX SAHB$_A$	ASTKKLSESLKXIGDXLDSN	FITC-βAla-	2614	872.7
BOK SAHB$_A$	RLAEVSAVLLXLGDXLEBIR	FITC-βAla-	2690	897.5
MCL-1 SAHB$_A$	KALETLRXVGDXVQRNHETAF	FITC-βAla-	2893	965.5
BCL-2 SAHB$_A$	VVHLTLRXAGDXFSRRY	FITC-βAla-	2499	834.0
BCL-X$_L$ SAHB$_A$	AVKQALRXAGDXFELRY	FITC-βAla-	2445	816.3
BCL-W SAHB$_A$	LHQABRXAGDXFETRF	FITC-βAla-	2370	791.2
BFL-1/A1 SAHB$_A$	KEVEKNLKXSLDXVNVVSV	FITC-βAla-	2609	870.8
Figure 2: Binding and specificity determinants of the MCL-1 BH3 helix.				
Figure 2a, 2b: MCL-1 SAHB$_A$ mutagenesis scan.				
MCL-1 SAHB$_A$	KALETLRXVGDXVQRNHETAF	FITC-βAla-	2893	965.5
MCL-1 SAHB$_A$K208A	AALETLRXVGDXVQRNHETAF	FITC-βAla-	2836	946.3
MCL-1 SAHB$_A$A209E	KELETLRXVGDXVQRNHETAF	FITC-βAla-	2951	984.4
MCL-1 SAHB$_A$L210A	KAAETLRXVGDXVQRNHETAF	FITC-βAla-	2851	951.5
MCL-1 SAHB$_A$E211A	KALATLRXVGDXVQRNHETAF	FITC-βAla-	2835	946.2
MCL-1 SAHB$_A$T212A	KALEALRXVGDXVQRNHETAF	FITC-βAla-	2863	955.3
MCL-1 SAHB$_A$L213A	KALETARXVGDXVQRNHETAF	FITC-βAla-	2851	951.5
MCL-1 SAHB$_A$R214A	KALETLAXVGDXVQRNHETAF	FITC-βAla-	2808	937.0
MCL-1 SAHB$_A$V216A	KALETLRXAGDXVQRNHETAF	FITC-βAla-	2865	956.2
MCL-1 SAHB$_A$G217A	KALETLRXVADXVQRNHETAF	FITC-βAla-	2907	970.2
MCL-1 SAHB$_A$G217E	KALETLRXVEDXVQRNHETAF	FITC-βAla-	2965	989.5
MCL-1 SAHB$_A$D218A	KALETLRXVGAXVQRNHETAF	FITC-βAla-	2849	950.8
MCL-1 SAHB$_A$V220A	KALETLRXVGDXAQRNHETAF	FITC-βAla-	2865	956.1
MCL-1 SAHB$_A$V220F	KALETLRXVGDXFQRNHETAF	FITC-βAla-	2941	981.6
MCL-1 SAHB$_A$Q221A	KALETLRXVGDXVARNHETAF	FITC-βAla-	2836	946.5
MCL-1 SAHB$_A$R222A	KALETLRXVGDXVQANHETAF	FITC-βAla-	2808	937.0
MCL-1 SAHB$_A$N223A	KALETLRXVGDXVQRAHETAF	FITC-βAla-	2850	951.0
MCL-1 SAHB$_A$H224A	KALETLRXVGDXVQRNAETAF	FITC-βAla-	2827	943.4
MCL-1 SAHB$_A$E225A	KALETLRXVGDXVQRNHATAF	FITC-βAla-	2835	946.0
MCL-1 SAHB$_A$T226A	KALETLRXVGDXVQRNHEAAF	FITC-βAla-	2863	955.6
MCL-1 SAHB$_A$A227E	KALETLRXVGDXVQRNHETEF	FITC-βAla-	2951	984.4
MCL-1 SAHB$_A$F228A	KALETLRXVGDXVQRNHETAA	FITC-βAla-	2817	940.2
Figure 2c: MCL-1 SAHB staple scan.				
MCL-1 BH3	KALETLRRVGDGVQRNHETAF	FITC-βAla-	2857	953.3
MCL-1 SAHB$_A$	KALETLRXVGDXVQRNHETAF	FITC-βAla-	2893	965.5
MCL-1 SAHB$_B$	KALXTLRXVGDGVQRNHETAF	FITC-βAla-	2821	965.5
MCL-1 SAHB$_C$	KALETLRRVXDGVXRNHETAF	FITC-βAla-	2921	974.8
MCL-1 SAHB$_D$	KALETLRRVGDGVXRNHXTAF	FITC-βAla-	2850	950.8
MCL-1 SAHB$_E$	KALETLRRVGDGVQRXHETXF	FITC-βAla-	2922	975.0
Figure 3: Crystal structure of the MCL-1 SAHB$_D$/MCL-1ΔNΔC complex.				
MCL-1 SAHB$_D$	KALETLRRVGDGVXRNHXTAF	Acetyl-βAla-	2502	835.0
Figure 4: MCL-1 SAHB$_D$ dissociates MCL-1/BAK and sensitizes BAK-dependent mitochondrial cytochrome *c* release.				
Figure 4a: BAK SAHB$_A$/MCL-1ΔNΔC competitive fluorescence polarization assay.				
BAK SAHB$_A$	QVGRQLAXIGDXINRRYD	FITC-βAla-	2583	862.0
MCL-1 BH3	KALETLRRVGDGVQRNHETAF	Acetyl-βAla-	2509	837.5
MCL-1 SAHB$_A$	KALETLRXVGDXVQRNHETAF	Acetyl-βAla-	2546	849.7
MCL-1 SAHB$_B$	KALXTLRXVGDGVQRNHETAF	Acetyl-βAla-	2474	825.5
MCL-1 SAHB$_C$	KALETLRRVXDGVXRNHETAF	Acetyl-βAla-	2574	859.2
MCL-1 SAHB$_D$	KALETLRRVGDGVXRNHXTAF	Acetyl-βAla-	2502	835.0
MCL-1 SAHB$_E$	KALETLRRVGDGVQRXHETXF	Acetyl-βAla-	2574	859.0
Figure 4b: Sensitization of BAK-dependent mitochondrial cytochrome *c* release.				
MCL-1 SAHB$_D$	KALETLRRVGDGVXRNHXTAF	Acetyl-βAla-	2502	835.0
BID BH3	DIIRNIARHLAQVGDSBDRSI	Acetyl-	2403	801.2
Figure 4c: Photoaffinity labeling of native MCL-1.				
MCL-1 SAHB$_D$	RKALETLRRVGDGVXRNHXTAF	Biotin-βAla-	2840	947.7
MCL-1 pSAHB$_D$	RKA**Bpa**ETLRRVGDGVXRNHXTAF	Biotin-βAla-	2980	994.5
Figure 4d: Dissociation of the native MCL-1/BAK interaction.				
MCL-1 SAHB$_D$	RKALETLRRVGDGVXRNHXTAF	Acetyl-βAla-	2659	887.1
Figure 5 and Supplementary Figure 6: Sensitization of caspase-dependent apoptosis.				
MCL-1 SAHB$_D$	RKALETLRRVGDGVXRNHXTAF	Acetyl-βAla-	2659	887.1
NOXA SAHB$_B$	LEVESXTQLXRFGDKLNFRQKL	Acetyl-	2710	904.4
BFL-1/A1 SAHB$_A$	KEVEKNLKXSLDXVNVVSV	Acetyl-βAla-	2260	754.3
MCL-1 SAHB$_D$	RKALETLRRVGDGVXRNHXTAF	FITC-βAla-	3005	1002.8
NOXA SAHB$_B$	LEVESXTQLXRFGDKLNFRQKL	FITC-βAla-	3130	1044.6
BFL-1/A1 SAHB$_A$	KEVEKNLKXSLDXVNVVSV	FITC-βAla-	2609	870.8

Amino acid nomenclature:

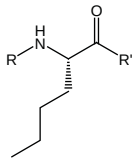

B: **L-norleucine**

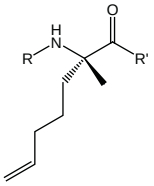

X: **(S)-2-(4'-pentenyl) alanine**

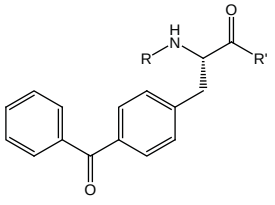

Bpa: **4-benzoyl-L-phenylalanine**

a

BCL-$X_L\Delta C$	K_D (nM)
MCL-1 $SAHB_A$	> 1000
NOXA $SAHB_A$	> 1000
BIM $SAHB_A$	1 ± 0.5
BID $SAHB_A$	28 ± 2
PUMA $SAHB_A$	9 ± 1
BAK $SAHB_A$	15 ± 3

b

BFL-1/A1ΔC	K_D (nM)
MCL-1 $SAHB_A$	>1000
NOXA $SAHB_A$	416 ± 172

Supplementary Table 2 (**a**) Dissociation constants for the interactions of MCL-1ΔNΔC-binding SAHBs with BCL-$X_L\Delta C$. Only MCL-1 and NOXA $SAHB_A$s displayed selectivity for MCL-1ΔNΔC versus BCL-$X_L\Delta C$ by FPA. Data are mean and s.d. for experiments performed in at least triplicate. (**b**) Dissociation constants for the binding interactions of MCL-1 and NOXA $SAHB_A$s with BFL-1/A1ΔC. Whereas NOXA $SAHB_A$ bound to BFL-1/A1ΔC, MCL-1 $SAHB_A$ was selective for MCL-1ΔNΔC, as measured by FPA. Data are mean and s.d. for experiments performed in at least triplicate.

Supplementary Table 3 Data collection and refinement statistics for the MCL-1 SAHB$_D$/MCL-1ΔNΔC crystal structure.

	MCL-1 SAHB$_D$/MCL-1ΔNΔC
Data collection	
Space group	P212121
Cell dimensions	
a, *b*, *c* (Å)	44.51, 56.87, 63.98
α, β, γ (°)	90, 90, 90
Resolution (Å)	42.51-2.32
R_{sym}	4.8 (38.4)[#]
$I / \sigma I$	13.6 (4.8)[#]
Completeness (%)	99.1 (100)[#]
Redundancy	7 (6.8)[#]
Refinement	
Resolution (Å)	42.51-2.32
No. reflections	7371
R_{work} / R_{free}	23.1/27.5
No. atoms	1351
Protein	1133
Ligand/ion	148
Water	70
B-factors	
Protein	85.0[*]
Ligand/ion	95.9[*]
Water	85.0[*]
R.m.s. deviations	
Bond lengths (Å)	0.002
Bond angles (°)	0.591

[#]Values in parentheses are for highest-resolution shell (2.42 Å - 2.32 Å).
[*]Total *B*-factor as defined by TLS refinement using PHENIX ($B_{total} = B_{tls} + B_{individual}$).

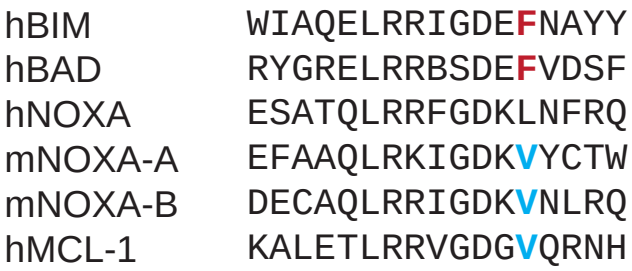

Supplementary Figure 1 Sequence alignment of select BH3 domains reveals key differences in core hydrophobic residues that engage the canonical BH3 pocket of anti-apoptotic proteins. The MCL-1 BH3 contains a unique LXXVGXXV motif. Both the BCL-2/BCL-X_L-selective BAD BH3 domain and the pan-anti-apoptotic binding BIM BH3 domain contain an F at the position corresponding to V220 in MCL-1 BH3. Interestingly, the murine NOXA BH3 domains, which exhibit selectivity for MCL-1, both contain a V in this position.

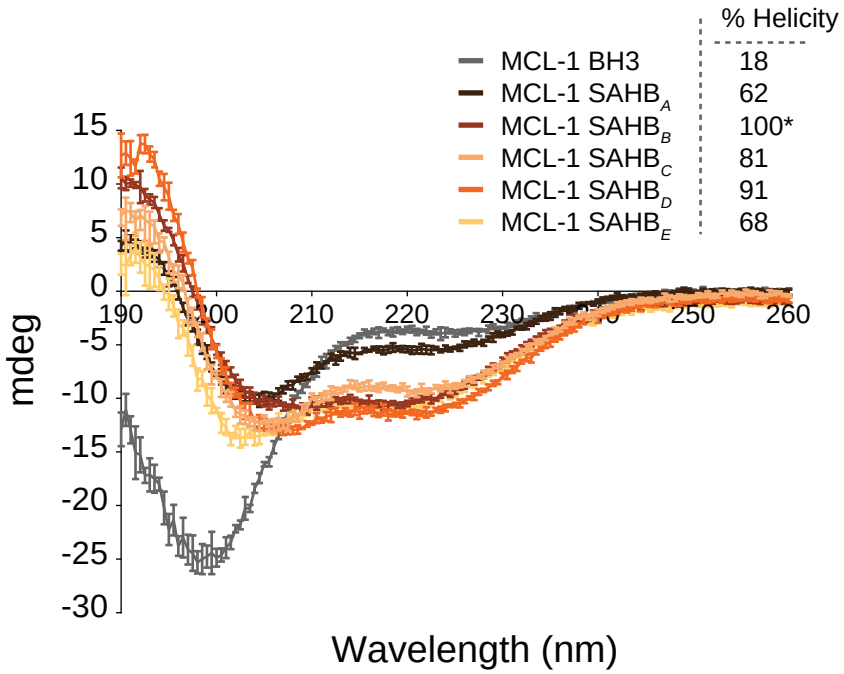

Supplementary Figure 2 Circular dichroism of MCL-1 SAHBs. MCL-1 SAHBs exhibit marked enhancement of α-helical structure compared to the corresponding unmodified peptide. The CD data are plotted as wavelength vs. millidegree. To estimate percent α-helicity, the precise peptide concentrations were confirmed by amino acid analysis, the CD data converted to mean residue ellipticity (θ), and α-helicity calculated as previously described[1,2]. Data are mean and s.d. for experiments performed in at least triplicate. *, exceeds the calculated ideal α-helicity for an undecapeptide standard[1,2].

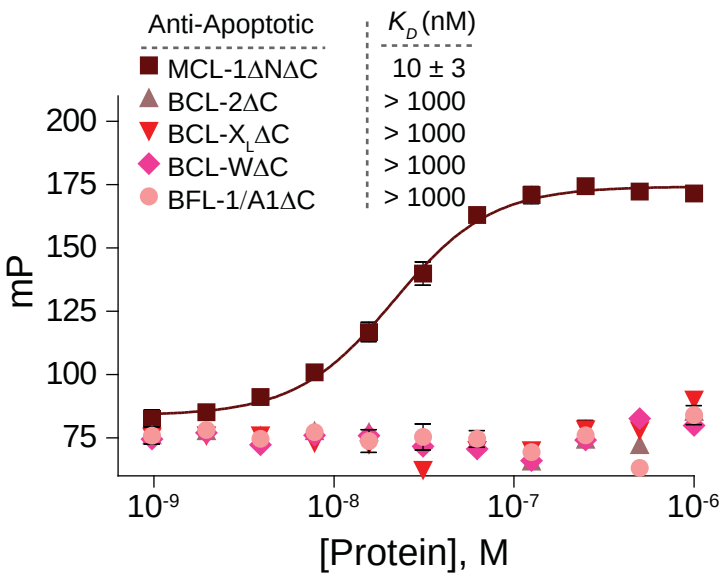

Supplementary Figure 3 MCL-1 binding specificity of MCL-1 $SAHB_D$. Like FITC-MCL-1 $SAHB_A$, FITC-MCL-1 $SAHB_D$ displayed a potent and exclusive interaction with MCL-1ΔNΔC, as evidenced by FPA performed against a broad panel of anti-apoptotic targets. Data are mean and s.d. for experiments performed in at least triplicate.

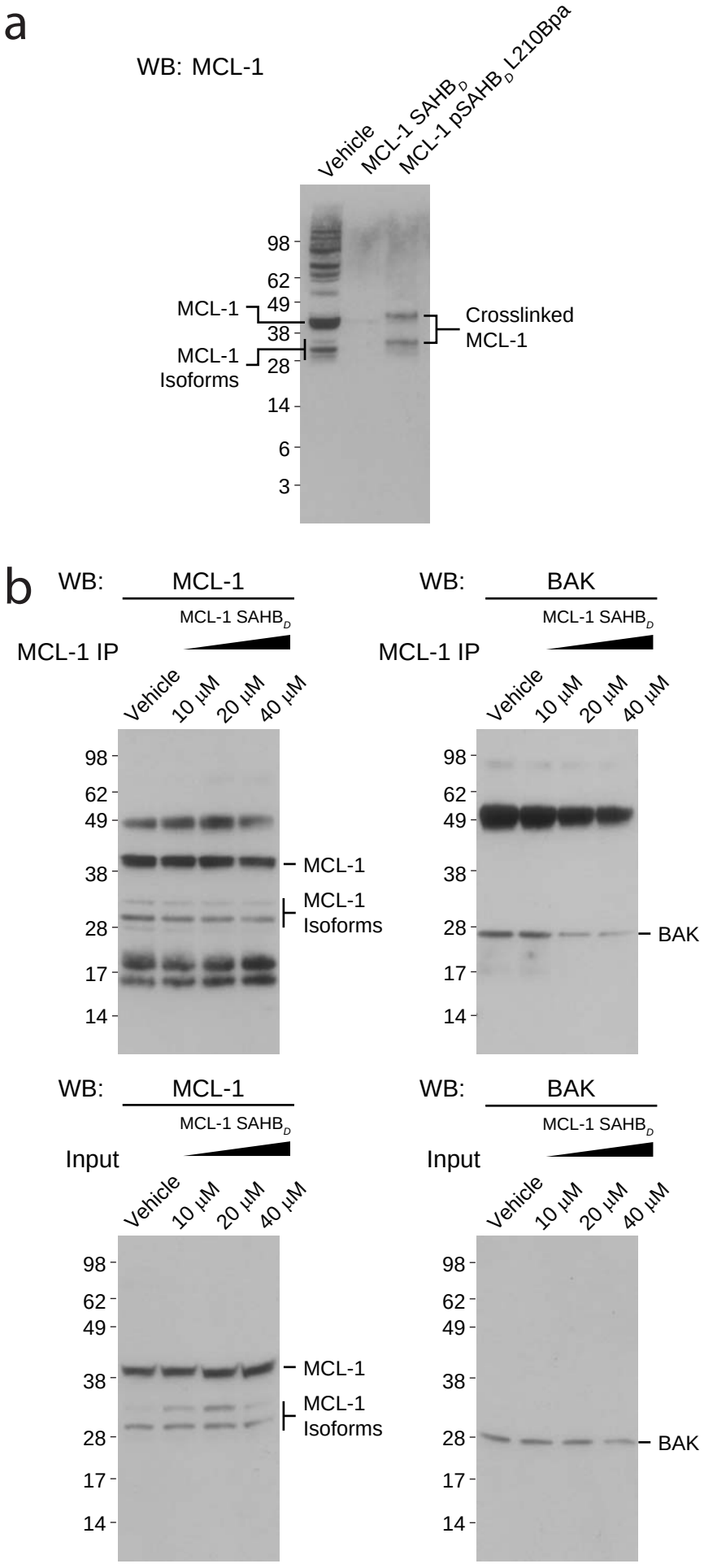

Supplementary Figure 4 MCL-1 SAHB photocrosslinking and MCL-1/BAK co-immunoprecipitation western analyses. (**a**) The photoreactive MCL-1 pSAHB$_D$, generated by replacing L210 with a benzophenone-bearing non-natural amino acid (Bpa), directly crosslinked to native MCL-1 within an OPM2 cellular lysate, whereas no covalent crosslinking was observed for MCL-1 SAHB$_D$, which lacked the photoreactive benzophenone moiety. The anti-MCL-1 S19 antibody specifically recognized the major cellular form of MCL-1 (~40 kD) and the less abundant lower molecular weight MCL-1 isoforms. The photocrosslinked MCL-1 pSAHB$_D$/MCL-1 species were correspondingly upshifted by a molecular weight of ~3 kD, which corresponds to the added mass of MCL-1 pSAHB$_D$. (**b**) The native interaction between BAK and MCL-1 was dose-responsively disrupted by treatment of OPM2 cells with MCL-1 SAHB$_D$, as assessed by MCL-1 immunoprecipitation and BAK western analysis. The anti-MCL-1 S19 antibody immunoprecipitated the major cellular form of MCL-1 (~40 kD) and the less abundant lower molecular weight MCL-1 isoforms from the OPM2 lysate; the heavy and light chains of immunoglobulin were also detected. The identical blot was stripped and reprobed with the BAK(NT) antibody and monomeric BAK was identified at ~28 kD. The MCL-1 and BAK bands were also detected in the corresponding input control blots. Vehicle, deionized water.

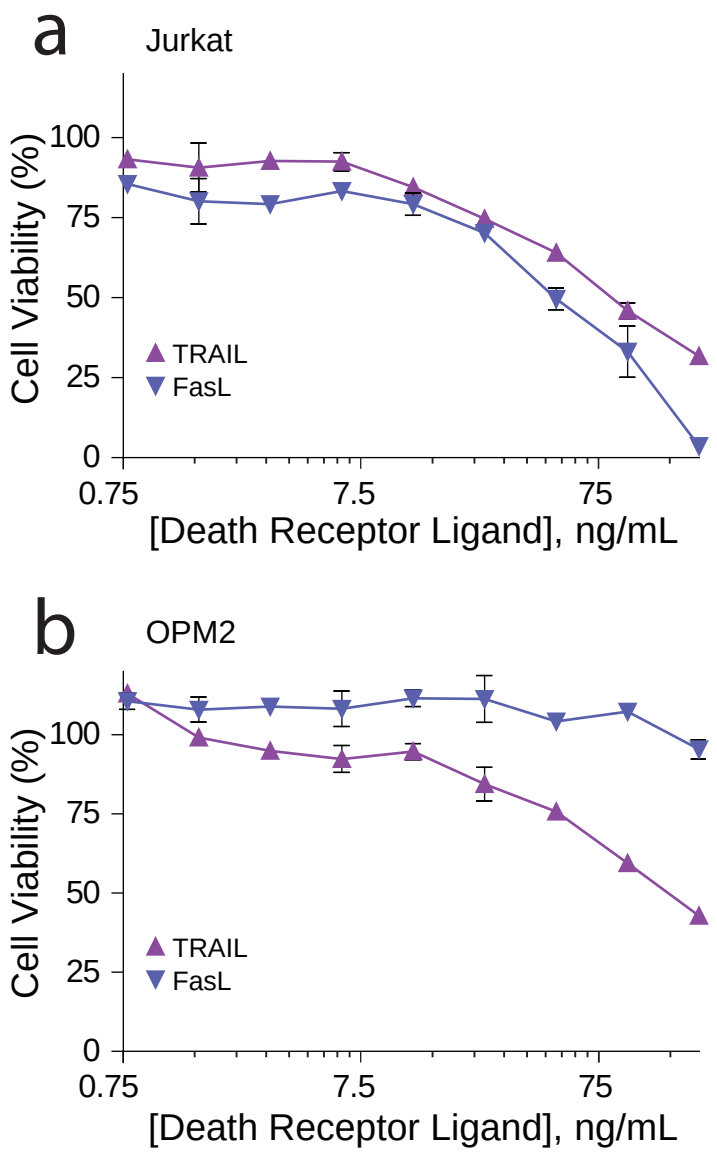

Supplementary Figure 5 Sensitivity of Jurkat and OPM2 cells to treatment with death receptor agonists. Jurkat and OPM2 cells were treated with increasing doses of TRAIL or Fas ligand (FasL), and cell viability was measured at 24 hours by MTT assay. Whereas TRAIL induced apoptosis of both Jurkat and OPM2 cells, only Jurkat cells were sensitive to FasL. Data are mean and s.d. for experiments performed in at least triplicate.

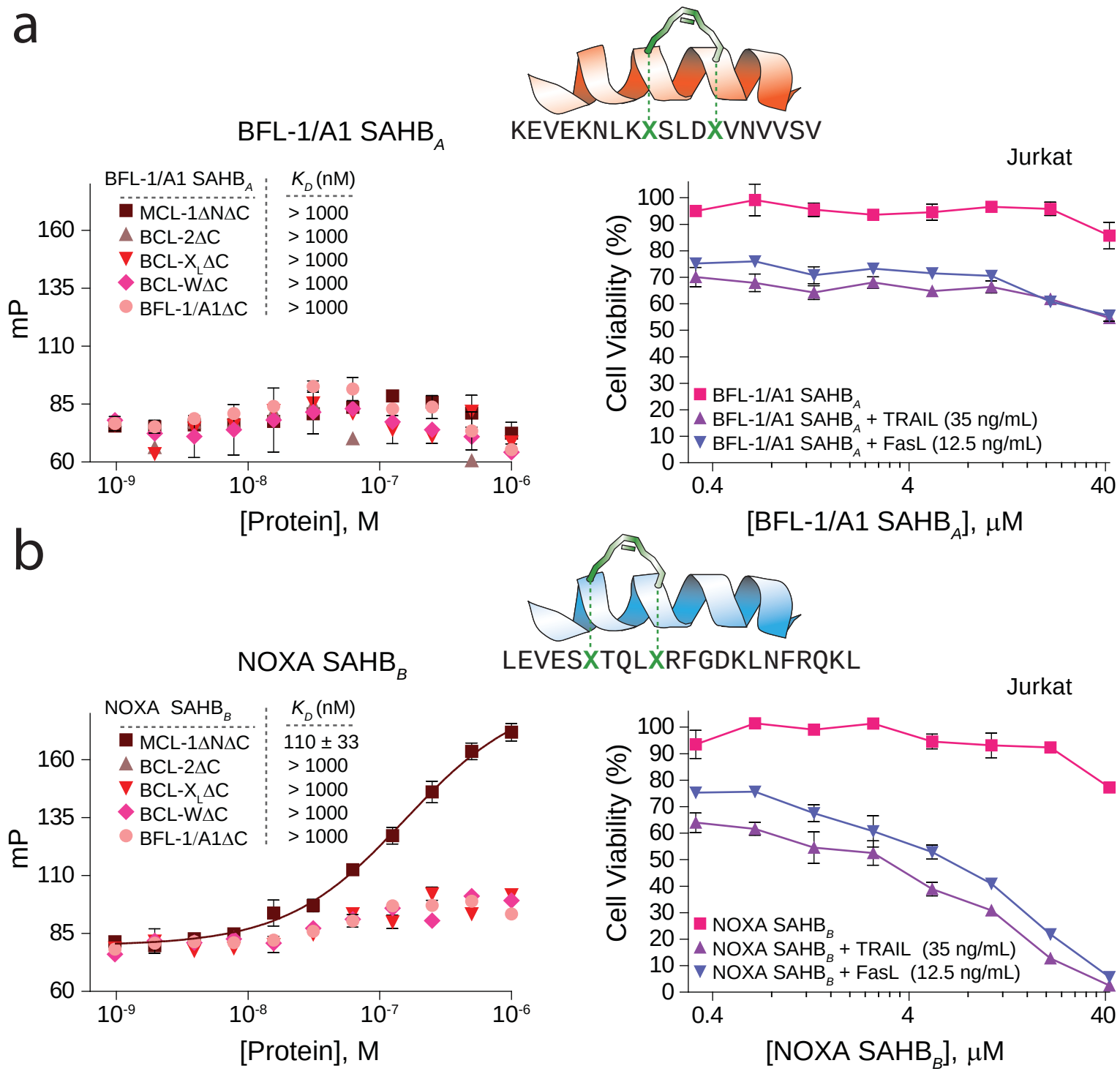

Supplementary Figure 6 Anti-apoptotic binding activity and apoptosis sensitization capacity of BFL-1 SAHB$_A$ and NOXA SAHB$_B$. (**a**) BFL-1 SAHB$_A$ exhibited no binding activity toward anti-apoptotic proteins by FPA and correspondingly showed no sensitization activity in Jurkat cells treated with low dose TRAIL or FasL. (**b**) Relocalizing the R31,K35 staple of NOXA SAHB$_A$ to position A26,R30 in NOXA SAHB$_B$ narrowed the natural MCL-1 and BFL-1/A1 binding selectivity of NOXA BH3 to MCL-1 only. Like MCL-1 SAHB$_D$, NOXA SAHB$_B$ sensitized the apoptotic response of Jurkat cells to TRAIL and FasL, as measured by MTT assay at 24 hours. (**c**) Lysates prepared from OPM2 cells treated with the indicated FITC-SAHBs contained similar intracellular levels of MCL-1 SAHB$_D$ and NOXA SAHB$_B$, whereas the negative control BFL-1/A1 SAHB$_A$ exhibited even greater cellular uptake. Binding and cellular data are mean and s.d. for experiments performed in at least triplicate. Vehicle, deionized water.

Stewart, et al. Figure S06

SUPPLEMENTARY REFERENCES

1. Bird, G.H., Bernal, F., Pitter, K. & Walensky, L.D. Chapter 22 Synthesis and biophysical characterization of Stabilized Alpha-helices of BCL-2 Domains. *Methods Enzymol* **446**, 369-86 (2008).
2. Forood, B., Feliciano, E.J. & Nambiar, K.P. Stabilization of alpha-helical structures in short peptides via end capping. *Proc Natl Acad Sci U S A* **90**, 838-42 (1993).